nature nanotechnology

LETTERS

PUBLISHED ONLINE: 1 DECEMBER 2014 | DOI: 10.1038/NNANO.2014.276

Ultrafast electronic readout of diamond nitrogen-vacancy centres coupled to graphene

Andreas Brenneis[1,2], Louis Gaudreau[3], Max Seifert[1], Helmut Karl[4], Martin S. Brandt[1], Hans Huebl[2,5], Jose A. Garrido[1,2], Frank H. L. Koppens[3]* and Alexander W. Holleitner[1,2]*

Non-radiative transfer processes are often regarded as loss channels for an optical emitter[1] because they are inherently difficult to access experimentally. Recently, it has been shown that emitters, such as fluorophores and nitrogen-vacancy centres in diamond, can exhibit a strong non-radiative energy transfer to graphene[2–6]. So far, the energy of the transferred electronic excitations has been considered to be lost within the electron bath of the graphene. Here we demonstrate that the transferred excitations can be read out by detecting corresponding currents with a picosecond time resolution[7,8]. We detect electronically the spin of nitrogen-vacancy centres in diamond and control the non-radiative transfer to graphene by electron spin resonance. Our results open the avenue for incorporating nitrogen-vacancy centres into ultrafast electronic circuits and for harvesting non-radiative transfer processes electronically.

With the advancement of nanoscale photonics research it has become increasingly desirable to combine optical systems with electric circuits to create optoelectronic devices that can be miniaturized and integrated into chips. To this end, we can take advantage of the excellent optical and electronic properties of graphene[9], which include good photodetection capabilities[8,10–15], efficient energy absorption[3] and strong light–matter interactions at the nanoscale[16,17]. In particular, it has been reported recently that, because of graphene's specific properties, the near-field interaction between light emitters and graphene is greatly enhanced as compared to that of conventional metals[2–6]. This interaction manifests itself, for example, in a 100-fold enhancement of the excited-state decay rate of emitters placed 5 nm away from graphene as compared to the spontaneous emission of the emitter. The physical mechanism behind the interaction is the creation of an electron–hole pair in graphene through non-radiative energy transfer (NRET) from the emitter dipole[18]. The NRET process to graphene has been demonstrated to have an efficiency of nearly 100% when the emitter is less than 10 nm away from the graphene sheet[3], which makes graphene an ideal material to detect electronically the optical properties of nearby emitters[6]. NRET has been studied extensively for fundamental as well as for biosensing applications. However, a fast energy transfer has not yet been observed because of quenching of the optical signal for short graphene-emitter distances. In contrast, an electronic readout of the NRET enables studies on fast energy processes. Moreover, if the transferred energy can be collected, as we show in this work, new ways for energy harvesting and biosensing can be implemented.

We take advantage of the highly efficient NRET process to read out electronically, for the first time, the optical excitation of nitrogen-vacancy (NV) centres in diamond nanocrystals. To this end, we used graphene for the extraction of the excited-state energy of NV centres and converted it into a measurable electrical signal. We chose NV centres as the optical emitters because of their outstanding characteristics in terms of robustness, stability, spin–photon coupling, ease of spin manipulation[19] and spin coherence, which have allowed them to play a fundamental role in new quantum technologies: room-temperature quantum registers based on the NV spin[20–22], spin–spin entanglement[23,24], spin–photon entanglement[25] and single-photon emitters[26], among others. Besides quantum-information processing, NV centres have also been used in metrology applications as extremely sensitive nanoscale magnetometers[27,28] and thermometers[29–31]. These applications require high photon-collection efficiencies and therefore bulky collection optics. Hence, an alternative method to extract the spin information from the NV centres is desirable. So far, the spin dynamics of NV centres have only been detected optically via fluorescence measurements. In this letter, we demonstrate the ultrafast on-chip electronic detection of NV spins.

Figure 1a shows the NRET process schematically. On optical excitation of the NV centre, the relaxation process occurs via NRET into the graphene, which generates an electron–hole pair. We detect the corresponding electronic excitations that originate from the NRET process by utilizing an Auston switch[7,8] that enables an on-chip ultrafast electronic readout with picosecond resolution (Fig. 1b inset and Methods). The measured current can be understood by considering the extra electron–hole pairs in the graphene, which are generated with a time rate that corresponds to the lifetime of the NV centres modified by the NRET. To verify that the current observed is caused by the non-radiative loss channel of the NV centres, we use the electron spin resonance (ESR) of the NV centres to modify the rate of NRET[32]. This change in rate induces a spin-dependent variation of the current in graphene.

Our device is configured as follows. A graphene sheet is coated with randomly distributed nanodiamonds (Fig. 2a), each containing ~500 NVs (Methods). Two gold striplines serve as electronic contacts to the graphene. We characterize the non-radiative transfer dynamics by measuring the current through the Auston switch when we activate it with a laser probe pulse at a time Δt after a laser pump pulse in the graphene region (inset of Fig. 1b and Methods)[8]. The circles in Fig. 2a highlight two positions in which nanodiamond clusters lie on top of graphene. At such positions, we detect a time-resolved current lasting for hundreds of picoseconds (blue-shaded part in Fig. 2b and Supplementary Figs 1 and 2). Figure 2c depicts a time-resolved current trace measured close to one of the metal contacts (triangle in Fig. 2a). At this position, the electric field is dominated by the built-in potential at the graphene–gold interface[8,14,15,33]. The long-lived transient currents (blue-shaded region in Fig. 2b,c) are caused by drift and diffusion of electron–hole pairs generated by NRET

[1]Walter Schottky Institut and Physik-Department, Technische Universität München, Am Coulombwall 4a, 85748 Garching, Germany. [2]Nanosystems Initiative Munich (NIM), Schellingstr. 4, 80799 Munich, Germany. [3]ICFO-Institut de Ciencies Fotoniques, Mediterranean Technology Park, 08860 Castelldefels, Barcelona, Spain. [4]Institute of Physics, University of Augsburg, 86135 Augsburg, Germany. [5]Walther-Meißner-Institut, Bayerische Akademie der Wissenschaften, 85748 Garching, Germany. *e-mail: frank.koppens@icfo.eu; holleitner@wsi.tum.de

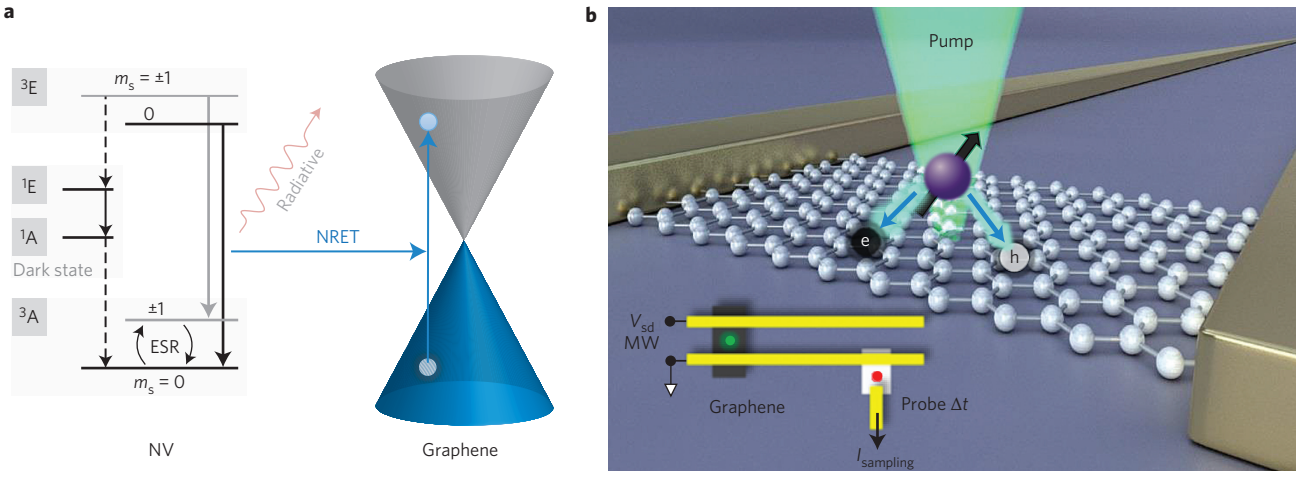

Figure 1 | Non-radiative readout scheme. a, The optically excited state of the NV centre with $m_s = 0, \pm1$ allows a NRET to the graphene (blue horizontal arrow). The optical excitation of the NV centre is spin conserving. However, the NV centre comprises a spin-selective metastable dark state ^{1}A, which offers an additional decay channel for $m_s = \pm1$ (dashed arrows) after a near-infrared (1,042 nm) radiative relaxation from ^{1}E. The ^{1}A state can thus reduce the NRET rate for the state $m_s = \pm1$ compared with the state $m_s = 0$. **b**, Excitations caused in the NV centre (purple sphere with a black arrow) can be transferred to the graphene via the NRET (blue arrows) and thus contribute to the current in the graphene. Two striplines act as near-field antennas and propagate all the currents as electromagnetic transients (inset). The transients are sampled at an ultrafast Auston switch with a time-delayed probe pulse (red circle). Thus, we can read out a d.c. current $I_{sampling}$ (Δt) for a fixed time delay Δt between the pump pulse and the probe pulse. The MW signal for the ESR is applied to the striplines.

from the NV centres and by direct optical absorption within the graphene. The excited electron–hole pairs directly generate a photoresponse[10] or decay into hot electrons and generate a photoresponse by the Seebeck effect[34]. The first peak at a time delay of $\Delta t \approx 0$ ps corresponds to an ultrafast displacement current within the graphene, that is, the screening of the local electric field caused by photogenerated charge carriers[7,8]. For a position without NV centres (rhomb, Fig. 2d), the detected transient currents are shorter in time, which is consistent with a photocurrent generated, for example, at the graphene–metal contact[8]. For each position, we plotted the long-lived transient currents for increasing time frames (Fig. 2e–g). We detected such long-lived currents at positions where clusters of nanodiamonds were located (for example, circles and triangles). In addition to the distribution of the NV centres, the transient-current map reflects the potential landscape within the graphene sheet. The long-lived currents have a timescale from picoseconds up to nanoseconds, which exceeds the direct laser-generated carrier dynamics in pristine graphene[8,14,15,33] (Supplementary Fig. 3). Also, the measured decay time is significantly shorter than the natural, characteristic lifetime of NV centres[18]. Therefore, these are signatures that the long-lived currents comprise the non-radiative transfer dynamics.

To verify that the long-lived contributions to $I_{sampling}$ stem from charge carriers from the NRET process, rather than from direct laser-light absorption, ESR provides a selective tool. To this end, we applied a microwave (MW) signal to the striplines (see the inset of Fig. 1b and Methods). The corresponding oscillating magnetic field can be tuned to the spin-splitting energy of the NV centres with a resonance at a MW frequency (f_{MW}) of 2.875 GHz (ESR in Fig. 1a)[19]. The energy spectrum of the NV centre contains a spin-triplet system with an $m_s = 0$ state and $m_s = \pm1$ degenerated states. On laser excitation the spin state of the system is conserved[19]. If the NV centre is in the $m_s = 0$ excited state, it decays radiatively with a characteristic lifetime of 10 ns to the $m_s = 0$ ground state. Conversely, if the NV centre is in the excited state $m_s = \pm1$, it can also decay via a dark state to the ground state $m_s = 0$ (Fig. 1a)[19]. The dark state has a lifetime in the order of hundreds of nanoseconds. This difference in decay rates between the $m_s = 0$ and $m_s = \pm1$ excited states is mapped via NRET onto the graphene by the creation of an electron–hole pair with corresponding probability. As our results indicate, the NRET process is less efficient when the NV centre is in the state $m_s = \pm1$ as compared with $m_s = 0$.

Figure 3a,b show $I_{sampling}$ for non-resonant and resonant ESR conditions (position of the dotted circle in Fig. 2a). For analysis, we fit the data with three contributions: a baseline I_{offset}, a Gaussian immediate response $I_{displacement}$ (red lines in Fig. 3a,b) and an exponentially decaying function I_{hot} (blue lines in Fig. 3a,b and Supplementary Fig. 2). I_{hot} describes the long-lived currents. We find that both I_{offset} and I_{hot} reduce under the spin-resonance conditions, but $I_{displacement}$ stays constant. The latter means that the local electric field at this position within the graphene and the displacement of the field are altered by neither the NRET nor the MWs. The component I_{hot} comprises transfer processes with a timescale of several picoseconds, and I_{offset} corresponds to a timescale of ~13 ns (the inverse of the repetition frequency of the laser, 76 MHz). When this offset component is plotted versus the f_{MW} and aliases of the laser repetition are subtracted (Supplementary Information), the resulting I^*_{offset} exhibits a clear dip at the ESR frequency (Fig. 3c and Supplementary Fig. 4), which is also observed for the component I_{hot} of the current (Fig. 3d, position of the triangle in Fig. 2a). This is consistent with standard ESR frequency-dependent photoluminescence measurements made on the same sample (Fig. 3e). The correspondence between the ESR dip measured optically and electronically is another clear demonstration of the NRET between the NV centre and the graphene. The NRET excites electron–hole pairs in the graphene, and therefore the current is temporarily increased in graphene. At the spin resonance, the relaxation channel through the dark state reduces the NRET, and therefore I_{hot} is reduced. Additional evidence to prove that the ESR signal originates from the NV centres is that, on excitation below the optical transition energy of NV centres, no ESR dip is observed (Fig. 3f).

We now focus our attention on the revealed timescales. The component I_{hot} shows two characteristic decay constants, τ_1 and τ_2 (Fig. 4a, Supplementary Fig. 2), that range from between a few picoseconds up to nanoseconds. The shorter time constant, τ_1, is approximately 40 ps and reflects the heat coupling of the graphene sheet to the substrate because this time constant is also detected in pristine graphene without nanodiamonds (Supplementary Fig. 3). In the regions away from the contacts, τ_1 also comprises the NRET dynamics because here the signal-to-noise ratio limits the detection of $I_{sampling}$ to shorter timescales (see Fig. 2b and Supplementary Fig. 3). Most strikingly, τ_2 significantly exceeds the decay times observed in pristine

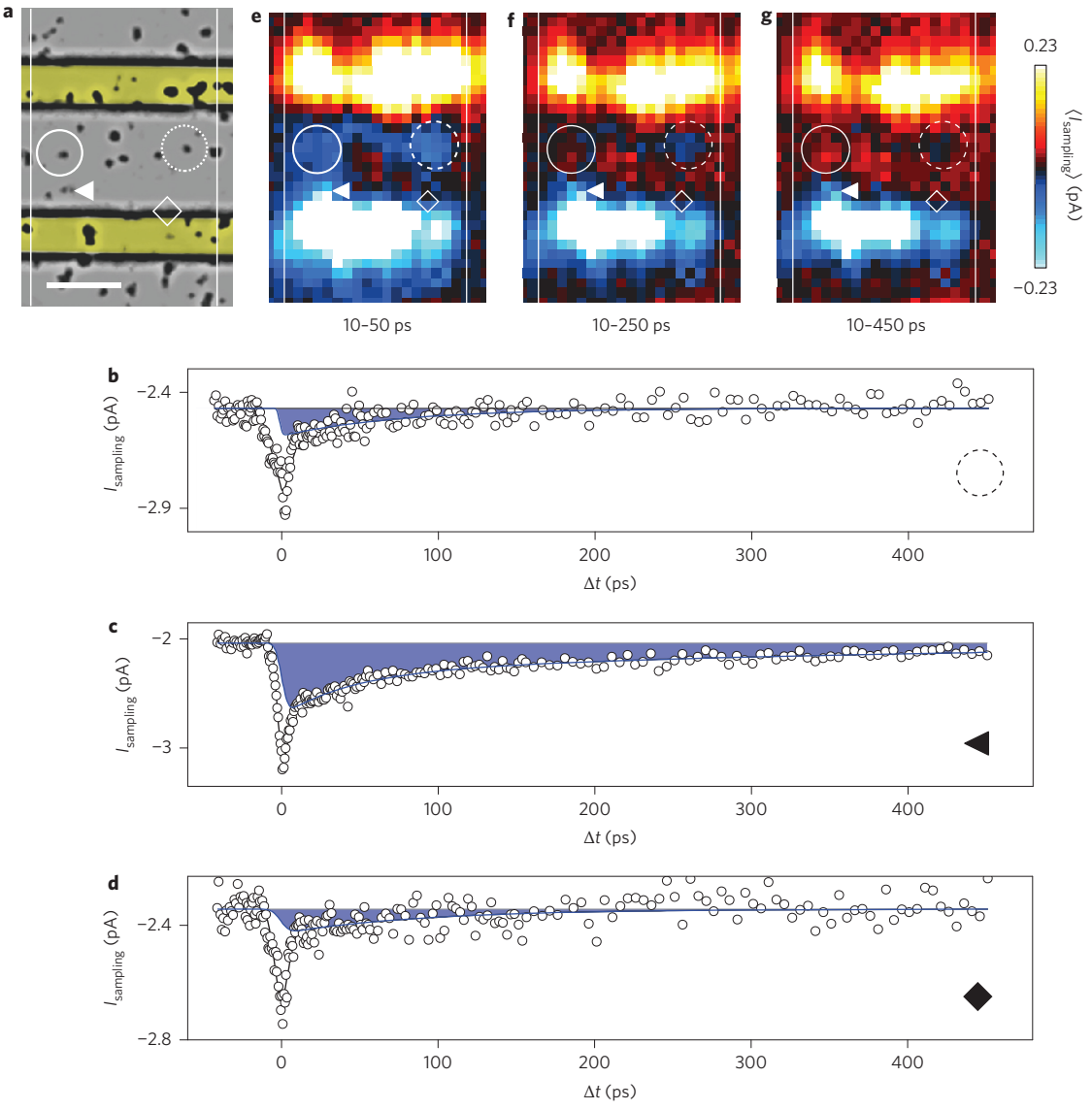

Figure 2 | Ultrafast electronic readout of NV centres. a, Graphene with diamond nanocrystals on top. White lines indicate the boundaries of the etched graphene sheet. Two metal striplines (yellow) act as source–drain contacts. Scale bar, 10 μm. **b**–**d**, Time-resolved current $I_{sampling}$ at positions marked by the dashed circle (**b**), triangle (**c**) and rhomboid (**d**) in **a**. **e**–**g**, Colour maps of the averaged long-lived currents as highlighted by the blue areas in **b** and **c** for time intervals Δt of 10–50 ps (**e**), 10–250 ps (**f**) and 10–450 ps (**g**). Experimental parameters are 77 K, P_{laser} = 3.0 mW, V_{sd} = 0 V.

graphene (Supplementary Fig. 3)[8]. To understand the longer decay times for the sample with nanocrystals, we need to discuss the dynamics of the NRET. Recently, it has been established, both theoretically and experimentally[2–4,6,17], that the near-field interaction between optical emitters and graphene leads to a dramatic reduction of the lifetime of the emitters depending on the distance that separates the emitter and the graphene sheet. Specifically, the lifetime τ_g of the emitter in the presence of graphene decreases as[3,4,17]:

$$\frac{\tau_0}{\tau_g} = 1 + \frac{9\nu\alpha}{256\pi^3(\epsilon+1)^2}\left(\frac{\lambda_0}{d}\right)^4 \quad (1)$$

where τ_0 is the natural lifetime of the emitter, α is the fine-structure constant, ε is the permittivity of the sapphire, d is the graphene-emitter distance, λ_0 is the emission wavelength and $\nu = 1$ or 2 if the emitter dipole is oriented parallel or perpendicular, respectively, to the graphene plane. For NV centres on a sapphire substrate ($\varepsilon = 3.12$) with an emission wavelength at 637 nm (zero phonon line)[18] and a natural lifetime of 10 ns, equation (1) results in a lifetime reduction from 10 ns at 50 nm to 77 ps at 5 nm (Fig. 4b). The physical mechanism of the NRET between an emitter and graphene is similar to the Förster resonant-energy transfer (FRET) between two coupled emitters through a near-field dipole–dipole interaction, but, contrary to FRET, the energy from the excited emitter is irreversibly transferred to the electronic excitations in graphene. The efficiency of the NRET is close to 100% for $d \leq 10$ nm (Fig. 4b). Comparing timescales, for $d > 50$ nm the long 10 ns lifetime of the NV centres is commensurate with the repetition frequency of the laser $1/f_{laser} = 76\ \mathrm{MHz}^{-1} \approx 13$ ns. This explains the role that I_{offset} plays in the electronic readout of the NRET. For I_{hot}, the decay times correspond to the reduction of the lifetime of the NV centres caused by the NRET. The different characteristic times for this decay reflect the distribution of lifetimes of the numerous NV centres with respect to their distance d. Indeed, owing to the size of the crystals (100 nm diameter) it is expected that the NRET is strongest for the NVs closest to the graphene sheet, and leads to decay times in the picosecond regime (Supplementary Fig. 3), and the NVs further away contribute less to the current

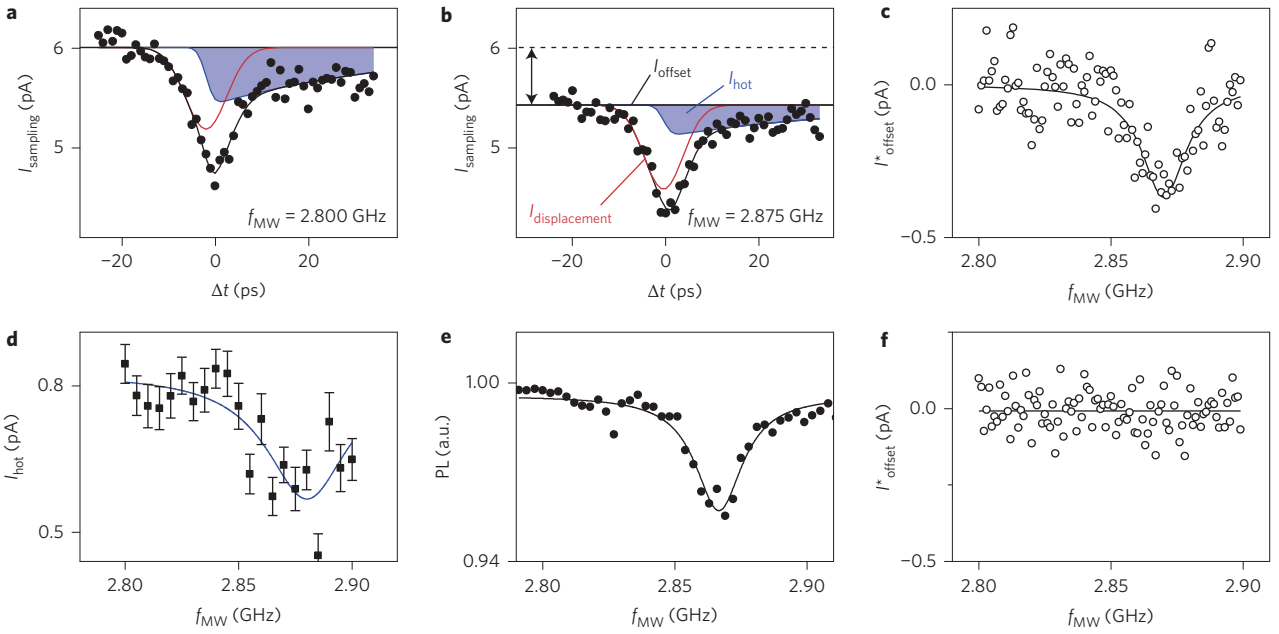

Figure 3 | Electronically and optically detected ESR. a, Time-resolved photocurrent under non-resonant MW irradiation excited at a position of nanodiamond clusters on the graphene. **b**, The signal can be characterized by an offset I_{offset} (horizontal line), a fast peak $I_{displacement}$ (red) and an exponentially decaying function I_{hot} (blue). I_{offset} and I_{hot} reduce under resonant MW irradiation. The double-headed arrow describes the ESR reduction of I_{offset} with respect to a non-resonant excitation (dashed line). **c**–**e**, I^*_{offset} (**c**), I_{hot} (**d**) and the photoluminescence versus f_{MW} with a dip at the spin-resonance frequency (**e**). **f**, The ESR signal of the current vanishes for a laser energy (1.53 eV per 811 nm) below the optical excitation energy of the NV centre. The experimental parameters for **a** and **b** are λ = 535 nm, P_{laser} = 2.0 mW, T_{bath} = 77 K, V_{sd} = 0.233 V, P_{MW} = 1 W; for **c** and **d**, λ = 535 nm, P_{laser} = 0.5 mW, T_{bath} = 77 K, V_{sd} = 0.233 V, P_{MW} = 1 W; for **e**, λ = 532 nm, P_{laser} = 2.0 μW, T_{bath} = 300 K, P_{MW} = 0.1 W; for **f**, λ = 811 nm, P_{laser} = 0.7 mW, T_{bath} = 77 K, V_{sd} = 0.233 V, P_{MW} = 1 W. a.u., arbitrary units.

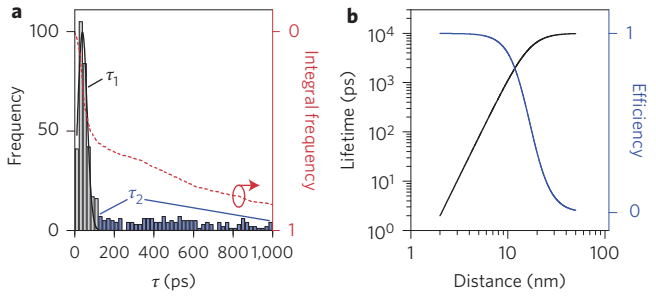

Figure 4 | Timescales of the non-radiative readout of NV centres. **a**, Frequency of prevailing time constants for all positions on the graphene sheet with nanocrystals on top and contributions $\tau_1 \approx 40$ ps and τ_2 up to nanoseconds. The dashed line is the integrated frequency over all delay times. **b**, Dependence of the lifetime on the distance between the NV and the graphene using equation (1). The lifetime is reduced by several orders of magnitude at short distances. The blue curve describes the efficiency of the NRET.

(Fig. 4b). Therefore, the long decay times observed in I_{hot} (compared to those in pristine graphene without crystals) reflect the NRET-decay rate of NVs close to graphene. As the measured characteristic times of I_{hot} are significantly shorter than the natural lifetime of the NV centres, the detected long-lived currents stem from a NRET process and not from NV fluorescence. Hereby, the measured current can be understood by extra electron–hole pairs in the graphene, generated at a time rate that corresponds to the lifetime of the NV centres modified by the NRET. Further verification of the electronic readout of the NV centres is given by the P_{MW} dependence and the P_{laser} dependence of the signal, which are consistent with the conventional optical detection of NV centres (Supplementary Fig. 4).

Conclusion

Our results show that the strong near-field interaction between graphene and optical emitters such as NVs in diamond can be harnessed to read out electronically the excited state of the emitters through NRET into electron–hole pair excitations in the graphene. The Auston-switch technology enables the electronic ultrafast detection (in timescales shorter than the natural lifetime of the NV centres) of these electronic excitations, which would otherwise be lost using the slower conventional electronics. To validate our conclusions, we induced ESR in the NV centres with resonant MWs. Contrary to conventional fluorescence measurements utilized to detect the spin state of the NV centres, our novel approach enables us to detect the ESR signal electronically, which gives access to characteristic lifetimes that range from the picosecond regime (for emitters closest to the graphene sheet) up to the natural lifetimes of NV centres in the nanosecond regime (for emitters further away from the graphene).

Generally, the nanodiamonds have a size of about 100 nm and they contain ~500 NV centres each. From integration of the transfer efficiency (Fig. 4b), we estimate that about ~16% (~80) of the NV centres within one nanodiamond contribute to the NRET current in the graphene. This number needs to be multiplied with the repetition frequency of the laser and the readout gain ($\sim 10^{-3}$) of the Auston switch, such that one can estimate a NRET current in the order of 1.0 pA, which is consistent with the amplitude of the measured current (see the Supplementary Information). The Auston-switch technology has a fundamental noise floor of about 2.0 fA (ref. 35). The noise floor of the presented measurements is in the order of 100 fA. It is dominated by the background noise of the optoelectronic set-up, including amplifiers operated at room temperature. In principle, it can be reduced by low-temperature amplification and further power stabilization of the laser to the fundamental noise floor. In turn, the readout of a single spin is technologically possible with the present technique. Our results pave the

way for alternative architectures of quantum technologies and metrology that combine the advantages of optical emitters, such as robustness, long coherence times at room temperature, and sensitivity, with on-chip integration into electronic circuits.

Methods

Fabrication of graphene. Graphene films were grown by chemical vapour deposition on copper foil in a hot-wall reactor. After preannealing the copper foil at 1,000 °C under a flow of 28 sccm H_2 for 40 minutes, graphene was grown for 30 minutes under a flow of 3.5 sccm CH_4 and 16 sccm H_2 at a total pressure of 10 mbar. Then, the copper–graphene foil was cooled to room temperature under a growth atmosphere. For transfer, samples were spin-coated with poly(methylmethacrylate) and floated on a 0.5 M aqueous $FeCl_3$ solution overnight. After complete dissolution of the copper foil, the films were rinsed with deionized water and transferred to the prestructured sapphire substrates with a stripline circuit on top.

Design of the stripline circuit. Sapphire with a thickness of 430 μm, covered with a 300 nm thick silicon layer, was used as a substrate. The silicon was implanted with O_2 ions to yield an excess carrier lifetime of ~1 ps. The silicon was etched in an initial lithographic step to define the ultrafast photoswitch (Auston switch), using HF/HNO_3 as the etchant. Ti (5 nm) and Au (25 nm) were evaporated to form the striplines and the readout contact of the Auston switch. The two striplines were 15 μm apart and they had a width of 5 μm. Each stripline had a total length of about 4.4 cm. The graphene was deposited on top of the striplines and defined to a 25 μm wide stripe in a final lithographic step by using O_2 plasma to remove the spare graphene. The distance between the graphene and the Auston switch was ~250 μm. The nanodiamonds had a diameter of ~100 nm and each comprised ~500 NVs (as provided by Adamas Nanotechnologies, Inc.). The nanodiamonds were spin-coated onto the circuit with an isopropanol solution. The same solvent was used for the pristine samples.

On-chip time-domain terahertz spectroscopy. A pulsed titanium:sapphire laser (repetition rate 76 MHz, pulse length 160 fs) operated at 811 nm was used for the probe pulse of the time-resolved measurements. The light was additionally converted by a nonlinear fibre into a wavelength of $\lambda = (535 \pm 5)$ nm, and focused as the pump laser onto the graphene with a ×10 objective. Each pump-laser pulse excited both graphene and the NV centres. The ultrafast currents in the graphene sheet were collected by the striplines. Consequently, an electromagnetic transient, which was proportional to the initial current, propagated along the striplines. After a certain time delay Δt, the probe pulse triggered the Auston switch and the presence of the electromagnetic transient drove an electric current, which decayed within 1 ps. This current was read out as $I_{\mathrm{sampling}}(\Delta t)$ and was proportional to the electric field of the propagating electromagnetic transient. The moment when the pump pulse hit the graphene defined $\Delta t \approx 0$ ps. Both laser beams were focused through the same objective on the sample, but the position of the pump beam on the graphene sheet could be scanned independently by a motorized mirror. The spot size of the pump beam was 3–4 μm. This beam had a power, P_{laser}, of 0.3–3 mW. The probe laser power was set to 100 mW. All laser powers were measured in front of the objective. We used a dual-frequency modulation of the pump and the probe beams, and for the readout the pre-amplified electric current I_{sampling} with a lock-in amplifier. For the readout of the Auston switch, we used an Ithaco 1211 with an integration time of milliseconds. The striplines were either connected to a voltage source-drain (V_{sd}) or connected via a bias tee to both an amplified MW source with power P_{MW} and the voltage source for ESR experiments. All measurements were done in a vacuum (10^{-5} mbar) at $T_{\mathrm{bath}} = 77$ K.

Received 30 May 2014; accepted 21 October 2014; published online 1 December 2014

References

1. Ford, G. W. & Weber, W. H. Electromagnetic interactions of molecules with metal surfaces. *Phys. Rep.* **113,** 195–287 (1984).
2. Gómez-Santos, G. & Stauber, T. Fluorescence quenching in graphene: a fundamental ruler and evidence for transverse plasmons. *Phys. Rev. B* **84,** 165438 (2011).
3. Gaudreau, L. *et al.* Universal distance-scaling of nonradiative energy transfer to graphene. *Nano Lett.* **13,** 2030–2035 (2013).
4. Swathi, R. S. & Sebastian, K. L. Long range resonance energy transfer from a dye molecule to graphene has (distance)$^{-4}$ dependence. *J. Chem. Phys.* **130,** 86101 (2009).
5. Velizhanin, K. A. & Shahbazyan, T. V. Long-range plasmon-assisted energy transfer over doped graphene. *Phys. Rev. B* **86,** 245432 (2012).
6. Koppens, F. H. L., Chang, D. E. & García de Abajo, J. F. Graphene plasmonics: a platform for strong light–matter interactions. *Nano Lett.* **11,** 3370–3377 (2011).
7. Auston, D. H. Impulse response of photoconductors in transmission lines. *IEEE J. Quant. Electron.* **19,** 639–648 (1983).
8. Prechtel, L. *et al.* Time-resolved ultrafast photocurrents and terahertz generation in freely suspended graphene. *Nature Commun.* **3,** 646 (2012).
9. Bonaccorso, F., Sun, Z., Hasan, T. & Ferrari, A. C. Graphene photonics and optoelectronics. *Nature Photon.* **4,** 611–622 (2010).
10. Xia, F., Mueller, T., Lin, Y-M., Valdes-Garcia, A. & Avouris, P. Ultrafast graphene photodetector. *Nature Nanotech.* **4,** 839–843 (2009).
11. Xu, X. *et al.* Photo-thermoelectric effect at a graphene interface junction. *Nano Lett.* **10,** 562–566 (2010).
12. Gabor, N. M. *et al.* Hot carrier-assisted intrinsic photoresponse in graphene. *Science* **334,** 648–652 (2011).
13. Song, J. C. W., Rudner, M. S., Marcus, C. M. & Levitov, L. S. Hot carrier transport and photocurrent response in graphene. *Nano Lett.* **11,** 4688–4692 (2011).
14. Sundaram, R. S. *et al.* The graphene–gold interface and its implications for nanoelectronics. *Nano Lett.* **11,** 3833–3837 (2011).
15. Sun, D. *et al.* Ultrafast hot-carrier-dominated photocurrent in graphene. *Nature Nanotech.* **7,** 114–118 (2012).
16. Chen, Z., Berciaud, S., Nuckolls, C., Heinz, T. F. & Brus, L. E. Energy transfer from individual semiconductor nanocrystals to graphene. *ACS Nano* **4,** 2964–2968 (2010).
17. Tisler, J. *et al.* Single defect center scanning near-field optical microscopy on graphene. *Nano Lett.* **13,** 3152–3156 (2013).
18. Liu, X. *et al.* Energy transfer from a single nitrogen-vacancy center in nanodiamond to a graphene monolayer. *Appl. Phys. Lett.* **101,** 233112 (2012).
19. Jelezko, F., Gaebel, T., Popa, I., Gruber, A. & Wrachtrup, J. Observation of coherent oscillations in a single electron spin. *Phys. Rev. Lett.* **92,** 76401 (2004).
20. Dutt, M. V. G. *et al.* Quantum register based on individual electronic and nuclear spin qubits in diamond. *Science* **316,** 1312–1316 (2007).
21. Neumann, P. *et al.* Multipartite entanglement among single spins in diamond. *Science* **320,** 1326–1329 (2008).
22. Fuchs, G. D., Burkard, G., Klimov, P. V. & Awschalom, D. D. A quantum memory intrinsic to single nitrogen-vacancy centres in diamond. *Nature Phys.* **7,** 789–793 (2011).
23. Pfaff, W. *et al.* Demonstration of entanglement-by-measurement of solid-state qubits. *Nature Phys.* **9,** 29–33 (2012).
24. Bernien, H. *et al.* Heralded entanglement between solid-state qubits separated by three metres. *Nature* **497,** 86–90 (2013).
25. Togan, E. *et al.* Quantum entanglement between an optical photon and a solid-state spin qubit. *Nature* **466,** 730–734 (2010).
26. Kurtsiefer, C., Mayer, S., Zarda, P. & Weinfurter, H. Stable solid-state source of single photons. *Phys. Rev. Lett.* **85,** 290–293 (2000).
27. Balasubramanian, G. *et al.* Nanoscale imaging magnetometry with diamond spins under ambient conditions. *Nature* **455,** 648–651 (2008).
28. Maze, J. R. *et al.* Nanoscale magnetic sensing with an individual electronic spin in diamond. *Nature* **455,** 644–647 (2008).
29. Acosta, V. M. *et al.* Temperature dependence of the nitrogen-vacancy magnetic resonance in diamond. *Phys. Rev. Lett.* **104,** 70801 (2010).
30. Plakhotnik, T. & Gruber, D. Luminescence of nitrogen-vacancy centers in nanodiamonds at temperatures between 300 and 700 K: perspectives on nanothermometry. *Phys. Chem. Chem. Phys.* **12,** 9751–9756 (2010).
31. Toyli, D. M., de las Casas, C. F., Christle, D. J., Dobrovitski, V. V. & Awschalom, D. D. Fluorescence thermometry enhanced by the quantum coherence of single spins in diamond. *Proc. Natl Acad. Sci. USA* **110,** 8417–8421 (2013).
32. Gruber, A. Scanning confocal optical microscopy and magnetic resonance on single defect centers. *Science* **276,** 2012–2014 (1997).
33. Freitag, M., Low, T., Xia, F. & Avouris, P. Photoconductivity of biased graphene. *Nature Photon.* **7,** 53–59 (2012).
34. Lemme, M. C. *et al.* Gate-activated photoresponse in a graphene p–n junction. *Nano Lett.* **11,** 4134–4137 (2011).
35. Auston, D. H., Johnson, A. M., Smith, P. R. & Bean, J. C. Picosecond optoelectronic detection, sampling, and correlation measurements in amorphous semiconductors. *Appl. Phys. Lett.* **37,** 371 (1980).

Acknowledgements

We thank A. Reserbat-Plantey for technical support. This work was supported by a European Research Council (ERC) Grant NanoREAL (No. 306754), the 'Center of NanoScience' in Munich and the DFG via SFB 631. L.G. acknowledges financial support from the Marie-Curie International Fellowship COFUND and ICFOnest program. F.H.L.K. acknowledges support from the Fundacio Cellex Barcelona, the ERC Career integration grant 294056 (GRANOP) and the ERC starting grant 307806 (CarbonLight).

Author contributions

A.B. and L.G. performed the experiments and analysed the data together with A.W.H., F.H.L.K., M.S., J.A.G., M.S.B., H.H., and H.K., and F.H.L.K. and A.W.H. conceived the study. All authors co-wrote the paper.

Additional information

Supplementary information is available in the online version of the paper. Reprints and permissions information is available online at www.nature.com/reprints. Correspondence and requests for materials should be addressed to F.H.L.K. and A.W.H.

Competing financial interests

The authors declare no competing financial interests.